



RESEARCH LETTER

10.1002/2014GL061491

Key Points:

- Subglacial meltwater flows upward through valley networks and freezes
- Both basal cooling and ridge line refreezing cause bedrock preservation
- The Gamburtsev Subglacial Mountains resemble younger midlatitude mountains

Supporting Information:

- Readme
- Text S1, Figures S1–S9, and Tables S1 and S2

Correspondence to:

T. T. Creyts,
tcreyts@ldeo.columbia.edu

Citation:

Creyts, T. T., et al. (2014), Freezing of ridges and water networks preserves the Gamburtsev Subglacial Mountains for millions of years, *Geophys. Res. Lett.*, *41*, 8114–8122, doi:10.1002/2014GL061491.

Received 9 AUG 2014

Accepted 13 OCT 2014

Accepted article online 17 OCT 2014

Published online 17 NOV 2014

This is an open access article under the terms of the Creative Commons Attribution License, which permits use, distribution and reproduction in any medium, provided the original work is properly cited.

Freezing of ridges and water networks preserves the Gamburtsev Subglacial Mountains for millions of years

Timothy T. Creyts¹, Fausto Ferraccioli², Robin E. Bell¹, Michael Wolovick¹, Hugh Corr², Kathryn C. Rose³, Nicholas Frearson¹, Detlef Damaske⁴, Tom Jordan², David Braaten⁵, and Carol Finn⁶

¹Lamont-Doherty Earth Observatory, Columbia University, Palisades, New York, USA, ²British Antarctic Survey, Cambridge, UK, ³School of Geographical Sciences, University of Bristol, Bristol, UK, ⁴Bundesanstalt für Geowissenschaften und Rohstoffe (BGR), Geozentrum Hannover, Hannover, Germany, ⁵Center for the Remote Sensing of Ice Sheets, Kansas University, Lawrence, Kansas, USA, ⁶U.S. Geological Survey, Denver Federal Center, Denver, Colorado, USA

Abstract Once an ice sheet grows beyond a critical thickness, the basal thermal regime favors melting and development of subglacial water networks. Subglacial water is necessary for bedrock erosion, but the exact mechanisms that lead to preservation of subglacial topography are unclear. Here we resolve the freezing mechanisms that lead to long-term, high-altitude preservation across the Gamburtsev Subglacial Mountains in East Antarctica. Analyses of a comprehensive geophysical data set reveal a large-scale water network along valley floors. The ice sheet often drives subglacial water up steep topography where it freezes along high ridges beneath thinner ice. Statistical tests of hypsometry show the Gamburtsevs resemble younger midlatitude mountains, indicating exceptional preservation. We conclude that the Gamburtsevs have been shielded from erosion since the latest Eocene (~34 Ma). These freezing mechanisms likely account for the spatial and temporal patterns of erosion and preservation seen in other glaciated mountain ranges.

1. Introduction

Continental ice sheets nucleate on mountain ranges through multiple glacial cycles [DeConto and Pollard, 2003; Marshall, 2002]. During warmer interglacial periods, these mountain ranges provide a toehold for snow accumulation and small glaciers that expand as temperatures drop. Mountain glaciers and periglacial processes tend to erode bedrock efficiently [Hallet et al., 1996; Shuster et al., 2011; Herman et al., 2011]. The switch from an erosive mountain glacier setting to a protective ice sheet setting requires a reduction of the sliding velocity by increasing coupling at the ice-bed interface. This precludes widespread sliding along the bed and reduces erosion.

Once an ice sheet grows beyond a critical size, its basal thermal regime favors melting and formation of subglacial water networks. Such water networks have been inferred to operate on short timescales [e.g., Fricker et al., 2007]. Complex subglacial thermal regimes that juxtapose warm-based, temperate areas against frozen, preserved regions have been interpreted on deglaciated beds [Kleman and Hättestrand, 1999; Sugden, 1978] but have never been imaged beneath a modern ice sheet.

Here we show how water networks develop and then freeze, causing ice sheet flow to be dominated by internal deformation instead of sliding. We analyze ice penetrating radar from the AGAP (Antarctica's Gamburtsev Province) aerogeophysical survey to measure ice thickness, determine subglacial topography, and map subglacial water distribution near Dome A, the highest point of the East Antarctic Ice Sheet (Figure 1). The Gamburtsev survey covers a region of approximately 250 × 750 km (section S1 in the supporting information).

Geologic records from the margins of the East Antarctic Ice Sheet suggest significant changes in the ice sheet margin since its inception. Immediately to the north of the Gamburtsevs along the Lambert-Amery margin, the ice sheet has waxed and waned through the late Oligocene and Miocene Climatic Optimum (~14–26 Ma). Global temperature proxies indicate that these were the warmest conditions during extensive Antarctic glaciation [Zachos et al., 2008] with some authors suggesting deglaciation in the Gamburtsevs in

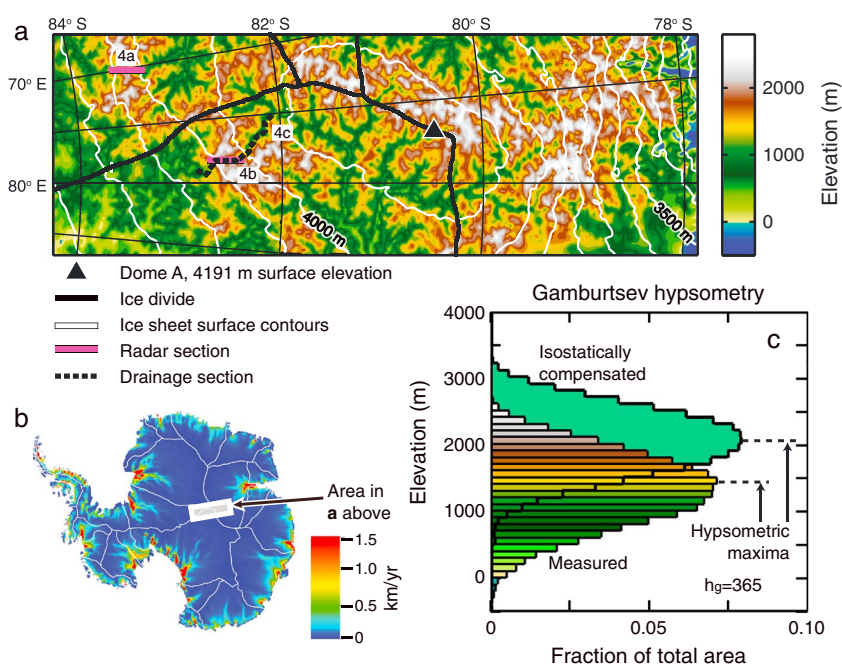


Figure 1. Gamburtsev Subglacial Mountains. (a) Bed topography from ice penetrating radar (section S1) and ice surface topography (white contours) [Bamber *et al.*, 2009]. (b) Balance velocity map of Antarctica [Budd and Warner, 1996] showing the area of the Gamburtsevs. Color scale indicates velocity magnitude. Intersecting ice drainage divides (thin white lines) indicate catchments of East Antarctica that source in the Gamburtsevs. (c) Hypsometry of the Gamburtsevs using radar data (with same color scale as in Figure 1a) and an Airy-compensated topography (solid green). Maximum bed elevations are 2768 m and 3361 m for measured and isostatically compensated beds, respectively. Hypsometric maxima, elevations with highest fraction of total area, are at ~ 1275 m and ~ 1975 m for measured and compensated beds, respectively. Mean elevations increase from 1351 m to 2070 m for measured and compensated beds, respectively, with an average isostatic uplift of 719 m. The parameter h_g gives the decay of an exponential fit to the hypsometry [Pedersen *et al.*, 2010] (section S4).

the Miocene [e.g., Bo *et al.*, 2009]. Moraines and glaciomarine deposits record this waxing and waning of the ice sheet [Hambrey *et al.*, 2007], and there appears to be a signal of contemporaneous isostatic peak uplift associated with late Cenozoic erosion along the Lambert Glacier to the north [Ferraccioli *et al.*, 2011].

Several independent observations support long-term preservation of the Gamburtsevs during the waxing and waning of the ice sheet. Erosional histories inferred from detrital thermochronologic data from Prydz Bay support low erosion rates [Thomson *et al.*, 2013], and offshore sediment thickness reconstructions suggest low overall erosion [Wilson *et al.*, 2012]. Simulations of a small ice sheet that covered the mountains through the Oligocene and Miocene indicate less erosive, cold-based ice [DeConto and Pollard, 2003; Jamieson *et al.*, 2010]. Additionally, the Gamburtsevs have a well-preserved glacial landscape as imaged by ground-based [Bo *et al.*, 2009] and airborne radars [Rose *et al.*, 2013]. In this study, we use the topography, in particular the broad-scale hypsometry, to demonstrate that the Gamburtsevs are relatively steep despite being tectonically inactive. We show that these observations suggest that preservation has occurred at least since the ice sheet formed in the early Oligocene (~ 34 Ma) and show how freezing beneath the ice sheet shields the bed from erosion.

2. Data and Methods

Data from multiple aerogeophysical sensors were collected using two Twin Otter aircraft over a 4 week period December 2008 to January 2009. The survey (120,000 line kilometers) was split into northern (AGAP-N) and southern (AGAP-S) sections. North-south survey lines were spaced approximately every 5 km with east-west lines intersecting every 33 km.

Here we focus on the results of the radar data. With variations that depend on flight velocity, the radar samples the ice at less than 2 m intervals along the flight track, but we resample the radar to approximately 16 m intervals. The radar footprint is approximately 1 km in the cross-track direction. The bed echo was picked

along the sharpest vertical gradient at the base of the ice sheet. Bed-returned power is determined from the brightest pixel within 50 m of that horizon. To identify water, we use two techniques. For the AGAP-N, water is identified through visual identification of continuous bright reflectors that lie along areas where the base of the ice sheet is flat. For AGAP-S, we identify water along the ice-bed interface using a hybrid technique of visual identification and anomalously bright radar reflectivity values (section S2) [Wolovick *et al.*, 2013].

To obtain subglacial topography from each radar line, we subtract the radar-derived ice thickness from ice surface topography [Bamber *et al.*, 2009]. Using the Geosoft Oasis montaj minimum curvature tool, we grid a digital elevation model (DEM) with 2.5 km grid spacing. We use this DEM to interpret regional-scale features, trends in topography, and subglacial water flow.

We also use hypsometry to compare the Gamburtsevs with midlatitude mountain ranges. Hypsometry is a histogram of elevation for a given area and is a method for evaluating topography at a large scale [Brozović *et al.*, 1997; Strahler, 1952]. We use only the radar-derived topography when calculating the hypsometry because minimum curvature gridding introduces artifacts between lines (sections S1 and S4). The total number of resampled radar data points used is 2,542,644. Our analysis focuses on the portion above the mode of the histogram. The mode is commonly referred to as the hypsometric maximum.

3. Results and Discussion

The Gamburtsevs are dissected by valley networks that are often not codirectional with present ice flow (Figures 1a and 1b) and therefore predate the present ice sheet. Gamburtsev peak and ridge elevations are over 2700 m above sea level and would rebound to over 3300 m if the ice sheet were removed. Large trunk valleys 250 km long and 10–25 km wide dominate the landscape. Where smaller tributaries join trunk valleys at higher elevations, very steep slopes indicate hanging valleys. Immediately below subglacial mountain ridges, large valley heads (5–20 km wide) occupy the highest bedrock elevations. Steep-sided valley walls, lower cirque levels, and overdeepenings along valley floors demonstrate that the entire range has been extensively modified by alpine-style glacial erosion [Rose *et al.*, 2013]. The large-scale hypsometry with a maximum at high elevation and a distribution that tapers from this maximum reflects an alpine morphology and is a characteristic signature of glacier erosion (Figure 1c) [Brozović *et al.*, 1997; Egholm *et al.*, 2009].

3.1. Water

Radar observations show concentrations of subglacial water bodies along deep valley axes. These are specular, mirror-like reflectors consistent with subglacial lakes that align in discrete bodies ranging from 100 to 8000 m long (mean length: 950 m, Figures 2a and 2b; Figure S5). In some cases, these specular reflections lie below internal layers that are deflected downward and suggest active melting of ice (Figure 3b). The water bodies are preferentially found beneath deep ice, and the water distribution drops off sharply under ice thinner than 2200 m (Figure 2b), suggesting that this is a minimum ice thickness necessary for basal meltwater generation.

A simple steady state water routing algorithm supports the location of water bodies along main flow paths (section S2). We route water down the hydraulic potential derived from topography,

$$\phi = \rho_w g z_b + \rho_i g (z_s - z_b), \quad (1)$$

where ρ_w and ρ_i are the densities of water and ice, z_s and z_b are bed and ice surface topography, and g is gravitational acceleration. In writing equation (1), we approximate the water pressure as equivalent to ice overburden pressure because the DEM grid scales are large relative to water depth at the ice-bed interface and water flow is far from an ice sheet boundary where atmospheric or submarine pressure conditions would affect the hydraulic system. Subglacial water flow algorithms represent an ersatz for a Darcian subglacial water flux q_w ,

$$q_w \propto -\nabla\phi, \quad (2)$$

by simply routing water down the hydraulic potential gradient (equation (1)). The water bodies identified from radar tend to align along inferred networks beneath thick ice. The correspondence of water observations and inferred pathways suggest that the algorithm describes subglacial water flow sufficiently.

From this analysis of flow directions, we find that there are two relationships between valley orientation and water flow. Where the valleys are aligned or nearly aligned with ice flow, water flows down the valleys

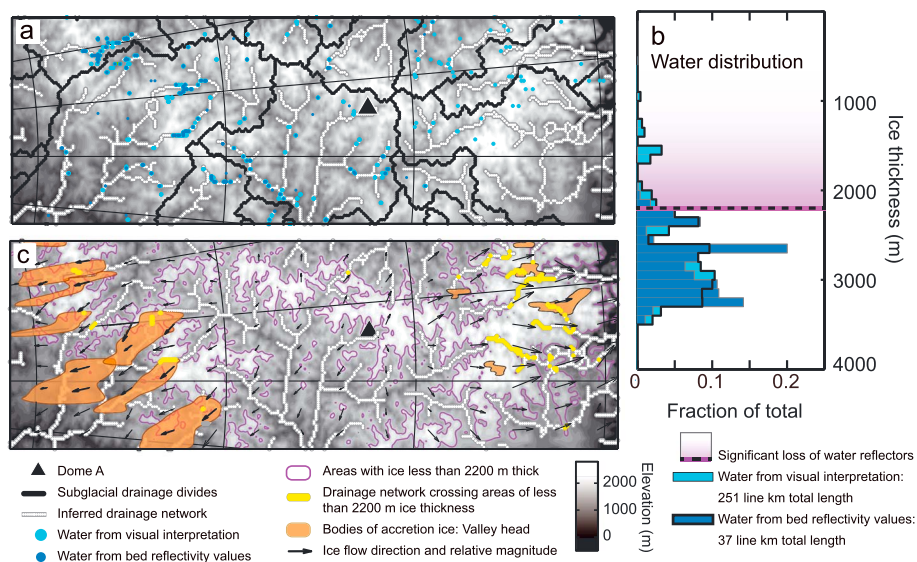


Figure 2. (a) Topography with water detected by radar. Bright radar returns relative to background are typically found along subglacial valley bottoms. Subglacial flow routes are often coincident with identified water. (b) Distribution of water with ice depth. Black dashed line indicates cutoff of 3% for visual interpretation and 8% for calculated residuals at 2200 m ice thickness with shaded area indicating very low water availability. The method of water identification gives a conservative estimate of its areal extent and is based on stringent thresholds. (c) Valley head reflectors of *Bell et al.* [2011] tend to originate in areas where water flow paths intersect ice thinner than 2200 m. Long continuous areas of subglacial water occur immediately upstream of thin ice (yellow dots). These are inferred thermal dams along flow paths. Subglacial water observations are coincident with the upstream accretion ice locations.

beneath progressively thicker ice including the main trunk valleys along the eastern margin (Figure 2a). However, along the southern and northern margins of the Gamburtsevs, the ice surface and bed slopes oppose each other, and water is driven up steep slopes toward thinner ice. Upward directed water flow is caused by the gradient of ice overburden pressure (second term in equation (1)) exceeding the gradient in gravitational potential attributable to bed topography (first term in equation (1)) [Cuffey and Paterson, 2010; Shreve, 1972]. These elevation gains are commonly thousands of meters and make these pathways striking examples of glacially driven uphill water flow.

On the upstream side of ridges, water collects in valley heads forming large, continuous bodies as indicated by numerous bright radar reflections (Figures 2a, 3c–3e, and S5). No water is found along network branches downstream of high ridges that are adverse to ice flow. This observation indicates discontinuities along water flow paths. These discontinuities extend 20–80 km downflow of the mountain peaks.

Spatially, the discontinuities in subglacial water correspond to areas where valley heads oppose ice flow and ice is thin (Figure 2a). These locations coincide with onset of basal ice plumes mapped in englacial radar data [Bell et al., 2011]. These basal ice plumes are relatively transparent with bed and englacial features clearly visible so that amounts of entrained sediment are insignificant.

We attribute loss of water reflectors to freezing under thin ice. Freezing creates thermal dams that prevent water flow across the mountains (Figures 2b, 3a, 3b, and 3e). The thermal dams cause the networks to back up, forming large water bodies that extend up valley beneath deeper ice. Where water drains through valleys that are aligned with ice flow, similar large water bodies are not observed, suggesting that water escapes the network. The disparity between the two types of networks indicates that the basal ice is largely frozen-on from the hydraulic system.

3.2. Basal Thermal Regime

Both development of water networks and basal freeze-on are controlled by the subglacial thermal regime. Near an ice dome, such as in the Dome A region, the thermal energy balance can be simplified to competition between geothermal heat flux and cold surface temperatures. Cold temperatures travel downward via advection with burial of surface snow or conduction of heat through the ice sheet [Cuffey and Paterson, 2010]. In the study area, accumulation of snow is low so that advection rates are comparable

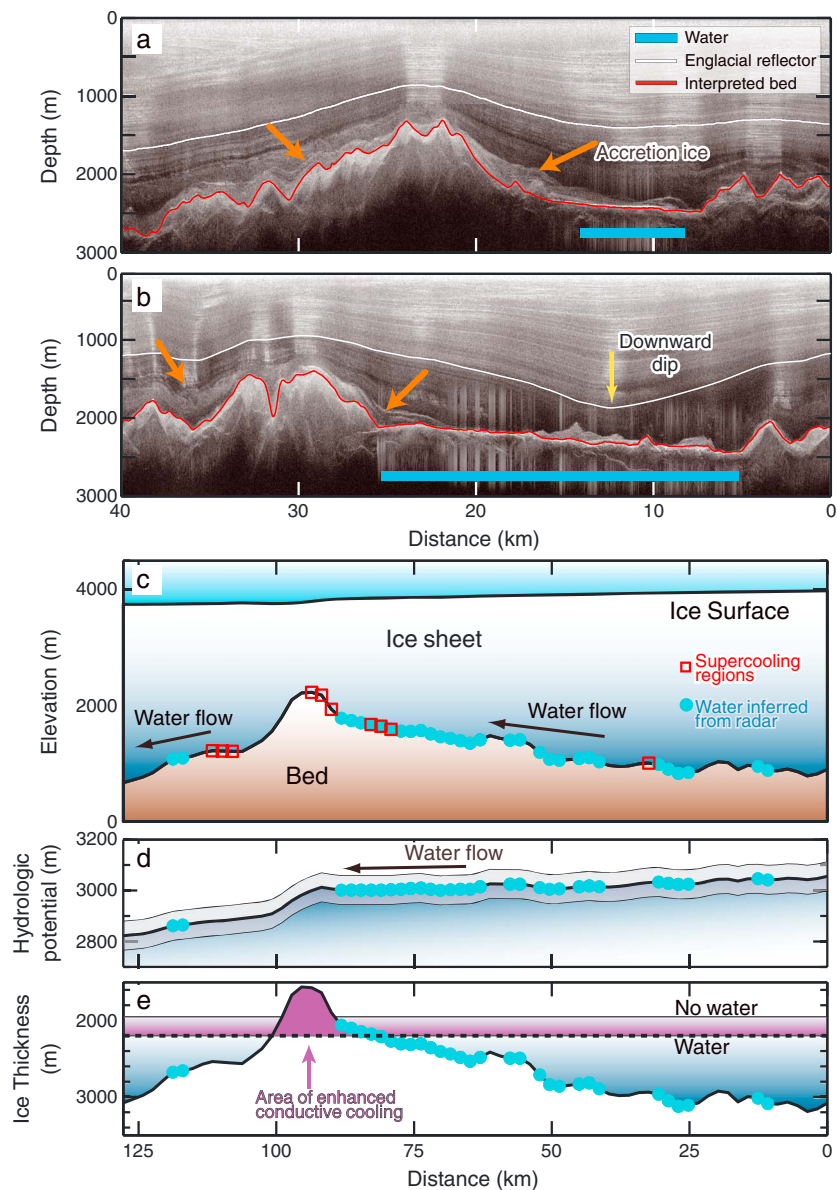


Figure 3. (a, b) Observations of water being dammed and frozen to the base of the ice sheet in two different valleys. Ice flow is right to left. In Figure 3b, the downward dip in the englacial reflectors indicates melt. (c) Data from a water flow path coincident with a portion of Figure 3b (see Figure 1a for overlap) shows that basal water inferred from radar reflections lies upstream in the valley. Supercooling regions meet or exceed the threshold for water freezing from ascending steep slopes. (d) Converting topography and ice thickness to hydrologic potential [Shreve, 1972] shows that water flowing down the hydrological potential would be driven over the mountain ridge. However, gradients are extremely low (errors indicated by the gray region in Figure 3d; section S2). (e) Thermal dams under thin ice (indicated by purple region) cause the water to pond upstream of the ridge and help preserve peak topography.

to or significantly less than conduction rates (section S3). The surface temperatures average -53°C and the geothermal heat flux is roughly $52 \pm 20 \text{ mW m}^{-2}$ [Shapiro and Ritzwoller, 2004]. Conduction is inversely proportional to ice thickness so that the peaks and ridges under thin ice are below the freezing point whereas the deep valleys are at the melting point. Along the peaks, heat loss calculations show fluxes of approximately 72 mW m^{-2} and exceed the geothermal heat flux (section S3). Thus, our observations of the spatial distribution of water bodies along valley bottoms and freeze-on ice along high topography are supported by simple but robust theoretical considerations.

Where the water networks are directed uphill, glaciohydraulic supercooling causes additional freezing and lessens the overall water budget. Glaciohydraulic supercooling occurs when the pressure-dependent melting point of flowing water drops and exceeds the heat added from other sources [Alley *et al.*, 1998; Creyts and Clarke, 2010]. Pressure decreases result from the decrease in ice overburden pressure along uphill-directed water flow. The scale of glaciohydraulic supercooling in the Gamburtsevs exceeds previous studies on glaciers [Hooke, 1991; Lawson *et al.*, 1998; Roberts *et al.*, 2002] by several orders of magnitude. Freeze-on along any individual flow path is, therefore, relatively long-lived. Because the heat sink is the water itself, glaciohydraulic supercooling does not change the temperature structure of the overlying ice. This effect means that lower thermal gradients through the ice can cause complete freezing of the networks.

3.3. Preservation of the Gamburtsevs

Two large-scale freezing patterns enable preservation of the highest elevations in the Gamburtsevs. The canonical frozen-bed regime occurs near domes, and ice divides where divergence of ice draws down cold surface temperatures to freeze the bed [Sugden, 1978; Cuffey and Paterson, 2010]. The canonical regime occurs over high bed topography where cold surface temperatures are moved downward beneath Dome A. The second regime occurs along peripheral ridges overlain by thin ice far from the core of the range. Here cold surface temperatures penetrate to the bed as ice flows over the ridges.

The interaction with basal water systems is different for these two regimes. In the canonical regime, water networks are directed away from the frozen-bedded areas. For the Gamburtsevs, these lie at the upstream end of the networks or have water networks flowing in valleys alongside the high topography. Where peripheral ridges are adverse to ice flow, uphill-directed water networks freeze where they meet colder temperatures. This “ridgeline refreezing” causes the thermal dams that back up the water system.

Freezing conditions over the ridges and peaks reduce or eliminate sliding and lower bedrock erosion. Because the slope of the hydraulic potential flattens as water ascends the ridges, water would tend to distribute over a wide area of the “interfluve” regions [Cuffey and Paterson, 2010] (Figure 3d and section S2). In these same areas, ice surface slopes steepen as ice moves over the mountains with locally enhanced ice velocities. The combination of distributed water and higher ice velocities would increase erosion. However, because of cold-bedded conditions, movement of ice preferentially is through internal deformation rather than basal sliding.

Bedrock erosion under cold-based ice below the freezing point is orders of magnitude slower than erosion beneath temperate ice at the pressure melting point [Cuffey *et al.*, 2000]. Bedrock plucking and abrasion are mainly controlled by sliding that requires water to decouple the ice from the bed and enhance stresses [Cohen *et al.*, 2006; Hallet, 1996]. Other processes that cause bedrock erosion, such as water pressure fluctuations [Hooke, 1991] or glaciofluvial erosion [Alley *et al.*, 1997], also require the presence of water and so are absent across frozen mountain ridges. Ridgeline freezing of the water networks therefore enables long-term protection of the peaks and ridges.

The freezing conditions along the ridges also have upstream effects that lessen erosion. Thermal dams reduce water flow gradients and cause development of subglacial lakes. The subglacial lakes reduce time-varying stresses on bedrock and lower water flow rates to suppress glaciofluvial erosion of loose bed materials. The lakes likely collect sediment that reduces bedrock exposure and also armors the bed.

The location of Dome A likely migrated over time in response to variations in accumulation rate across the region as shown, for example, in Greenland [Marshall and Cuffey, 2000]. The change in surface slope and orientation would alter flow directions of the subglacial water network. Thus, the locations of thermal dams and ridge line refreezing shift with migration of the dome. Similarly, the locations of canonical freezing through divergent ice flow would also migrate. The integrated effects are to preserve the ridges regardless of the location of the dome or direction of the water networks.

3.4. Hypsometry

We compare the characteristic alpine glacial hypsometry to contextualize the Gamburtsevs relative to other glaciated ranges [Pedersen *et al.*, 2010; Brozović *et al.*, 1997] and examine the extent of preservation. Glaciated mountain ranges commonly contain ice fields that are a contiguous group of glaciers separated by exposed ridges and peaks. The Gamburtsevs are unusual because they are completely covered by ice averaging ~2400 m thick. Other ranges had large fractions glaciated over the Plio-Pleistocene but none continuously covered by an ice sheet.

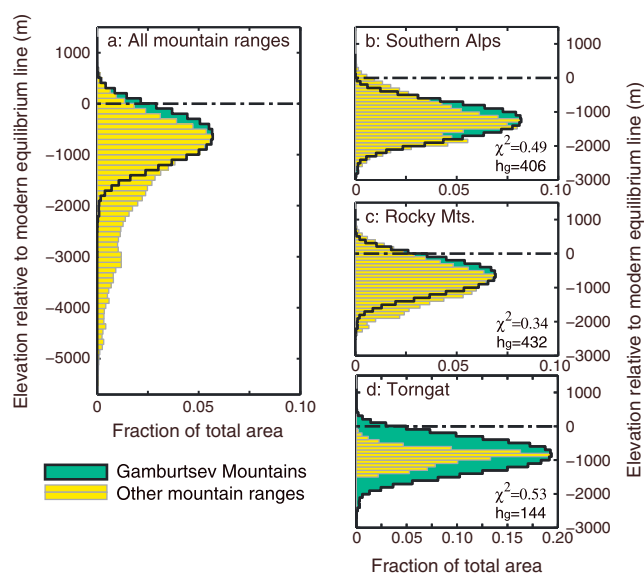


Figure 4. Hypsometry of the Gamburtsev Subglacial Mountains relative to other mountain ranges [Pedersen *et al.*, 2010]. (a) All mountains between 60°N and 60°S. Elevations are relative to the local equilibrium line altitude. (b) Southern Alps, New Zealand. (c) Rocky Mountains, USA. (d) Torngat Mountains, northern Canada. The hypsometry of the Gamburtsevs resembles younger mountain ranges such as the Southern Alps (rank = 5) and Rocky Mountains (rank = 3) but is dissimilar to older mountains such as the Torngats (rank = 10). Rankings are based on χ^2 and h_g fit parameters. (Table S2).

mountains based on rankings of the two metrics (Figures 4b and 4c and Table S2). Uplift of the Gamburtsevs, however, is significantly older [Cox *et al.*, 2010; Ferraccioli *et al.*, 2011; Thomson *et al.*, 2013] than those more recent ranges (section S4). The ranked order of the hypsometries does not fully distinguish between the two youngest classes of mountains. However, the Gamburtsevs do not resemble the older, inactive ranges. Based on these metrics, the steep and high glacial hypsometry of the Gamburtsevs is consistent with exceptional preservation.

We attribute this remarkable preservation of the Gamburtsevs to the basal thermal regime of the overlying East Antarctic Ice Sheet that nucleated there roughly 34 Ma ago [Zachos *et al.*, 2001]. Model results indicate that the Gamburtsevs remained completely covered by a smaller and regionally cold-based East Antarctic Ice Sheet even through the intervening and warmer Oligocene and Miocene periods [DeConto and Pollard, 2003; Jamieson *et al.*, 2010]. Even a smaller East Antarctic Ice Sheet would support melting of basal ice in the deep valleys, development of basal water networks, and freeze-on processes along high ridges similar to the processes presently active. We hypothesize that both basal freezing processes were the norm for millions of years beneath this part of the East Antarctic Ice Sheet. Our proposed mechanisms help explain the remarkable preservation of the Gamburtsevs and their apparent similarities to younger mountain ranges.

4. Summary and Conclusions

We propose that two freezing processes enable the remarkable subglacial preservation of the high-elevation mountain ridge topography of the Gamburtsevs. In addition to the canonical basal freezing processes from divergence of ice flow near ice domes and ice divides [Sugden, 1978], ridgeline freezing of subglacial water networks helps explain the spatial heterogeneity of preserved landscapes, while also allowing transfer of refrozen water from deep warmer interior regions to more cold-based areas with thinner ice cover. Evidence from past ice sheets, such as the Fennoscandian and Laurentide Ice sheets, indicate a geologic record of cold-based, preserved surfaces often juxtaposed with temperate, modified areas that supported basal water [Staiger *et al.*, 2005; Sugden, 1978]. For the Gamburtsevs, the irregular pattern of preservation conforms roughly to an ice-thickness depth rather than a topographic contour.

We use two metrics to assess the Gamburtsevs relative to a recent global compilation of glaciated ranges [Pedersen *et al.*, 2010]. The first metric is a χ^2 goodness-of-fit test that measures the relative scaled mass of the mountain ranges above the hypsometric maximum. The second metric follows Pedersen *et al.* [2010] and results from an exponential fit to the highest portion of the hypsometry (section S4). The χ^2 test is a fit of mass to areal extent, and the exponential fit is a test of steepness. The two metrics are independent, sampling different qualities of the hypsometries (Figure S8). Our analysis focuses on topography above the hypsometric maximum (~1275 m, Figure 1c) because our survey does not adequately sample the piedmont.

Global hypsometry is dominated by the young and massive ranges, such as the Himalaya-Tibet region and the Andes (Figure 4a) [Pedersen *et al.*, 2010]. The Gamburtsevs retain much of their mass and bear striking resemblance to active and recently active moun-

Similar observations from deglaciated beds may yield insight into past ice sheet thermal regimes and basal hydrology.

The preservation of other mountain ranges that provided major nucleation centers for former Plio-Pleistocene ice sheets [DeConto and Pollard, 2003; Marshall, 2002] may also be similarly linked to spatially variable basal thermal regimes. Despite enhanced bedrock erosion during ice sheet expansion [Molnar, 2004], the peaks and ridges of the Torngat Mountains in northern Canada [Sugden, 1978; Staiger et al., 2005], the Scandinavian Mountains [Sugden, 1978], and the high ridges of the Patagonian Andes are also well preserved [Thomson et al., 2010]. By preserving these nucleation centers, ice sheets are able to grow repeatedly and rapidly by self-regulating their regional conditions before expanding to influence global climate cycles [DeConto and Pollard, 2003].

Acknowledgments

We thank field party members of the AGAP research campaign. We thank V.K. Pedersen and D.L. Egholm for providing hypsometric data for global mountain ranges. Members of Center For Remote Sensing of Ice Sheets (CREGIS) kindly provided algorithms and data products used during this analysis. We are grateful to R. Alley, M. Fahnestock, G. Flowers, and C. Schoof for reviews of early versions of this manuscript. We are grateful for the help of H. Abdi with figure preparation. Radar data are served online by L-DEO and BAS. The resultant ice thickness data have been incorporated into BEDMAP2 project and are served online by BAS. We thank Stuart Thomson and an anonymous referee for constructive comments on this manuscript. This work was made possible through support from the U.S. NSF Polar Program, UK NERC, and the Federal Institute for Geosciences and Resources, Germany.

We thank Stuart Thomson and an anonymous referee for constructive comments on this manuscript.

References

- Alley, R. B., K. M. Cuffey, E. B. Evenson, J. C. Strasser, D. E. Lawson, and G. J. Larson (1997), How glaciers entrain and transport basal sediment: Physical constraints, *Quat. Sci. Rev.*, *16*, 1017–1038.
- Alley, R. B., D. E. Lawson, E. B. Evenson, J. C. Strasser, and G. J. Larson (1998), Glaciohydraulic supercooling: A freeze-on mechanism to create stratified, debris-rich basal ice: II. Theory, *J. Glaciol.*, *44*(148), 563–569.
- Bamber, J. L., J. L. Gomez-Dans, and J. A. Griggs (2009), A new 1 km digital elevation model of the Antarctic derived from combined satellite radar and laser data – Part 1: Data and methods, *Cryosphere*, *3*(1), 101–111.
- Bell, R. E., et al. (2011), Widespread persistent thickening of the East Antarctic Ice Sheet by freezing from the base, *Science*, *331*, 1592–1595, doi:10.1126/science.1200109.
- Bo, S., M. J. Siegert, S. M. Mudd, D. Sugden, S. Fujita, C. X. J. Yunyun, T. Xueyuan, and L. Yuansheng (2009), The Gamburtsev Mountains and the origin and early evolution of the Antarctic Ice Sheet, *Nature*, *459*, 690–693, doi:10.1038/nature08024.
- Brozović, N., D. W. Burbank, and A. J. Meigs (1997), Climatic limits on landscape development in the Northwestern Himalaya, *Science*, *276*(5312), 571–574.
- Budd, W. F., and R. C. Warner (1996), A computer scheme for rapid calculations of balance-flux distributions, *Ann. Glaciol.*, *23*, 21–27.
- Cohen, D., T. S. Hooyer, N. R. Iverson, J. F. Thomason, and M. Jackson (2006), Role of transient water pressure in quarrying: A subglacial experiment using acoustic emissions, *J. Geophys. Res.*, *111*, F03006, doi:10.1029/2005JF000439.
- Cox, S. E., S. N. Thomson, P. W. Reiners, S. R. Hemming, and T. van de Fliedert (2010), Extremely low long-term erosion rates around the Gamburtsev mountains in interior East Antarctica, *Geophys. Res. Lett.*, *37*, L22307, doi:10.1029/2010GL045106.
- Creyts, T. T., and G. K. C. Clarke (2010), Hydraulics of subglacial supercooling: Theory and simulations for clear water flows, *J. Geophys. Res.*, *115*, F03021, doi:10.1029/2009JF001417.
- Cuffey, K. M., and W. S. B. Paterson (2010), *The Physics of Glaciers*, 4th ed., 693 pp., Butterworth-Heinemann/Elsevier, Burlington, Mass.
- Cuffey, K. M., H. Conway, A. M. Gades, B. Hallet, R. Lorrain, J. P. Severinghaus, E. J. Steig, B. Vaughn, and J. W. C. White (2000), Entrainment at cold glacier beds, *Geology*, *28*(4), 351–354.
- DeConto, R. M., and D. Pollard (2003), Rapid Cenozoic glaciation of Antarctica induced by atmospheric CO₂, *Nature*, *421*, 245–249, doi:10.1038/nature01290.
- Egholm, D. L., S. B. Nielsen, V. K. Pedersen, and J. Lesemann (2009), Glacial effects limiting mountain height, *Nature*, *460*, 884–888, doi:10.1038/nature08263.
- Ferraccioli, F., C. A. Finn, T. Jordan, R. E. Bell, L. M. Anderson, and D. Damaske (2011), East Antarctic rifting triggers uplift of the Gamburtsev mountains, *Nature*, *479*, 388–392, doi:10.1038/nature10566.
- Fricter, H. A., T. Scambos, R. Bindshadler, and L. Padman (2007), An active subglacial water system in West Antarctica mapped from space, *Science*, *315*(5818), 1544–1548, doi:10.1126/science.1136897.
- Hallet, B. (1996), Glacial quarrying: A simple theoretical model, *Ann. Glaciol.*, *22*, 1–8.
- Hallet, B., L. Hunter, and J. Bogen (1996), Rates of erosion and sediment evacuation by glaciers: A review of field data and their implications, *Global Planet. Change*, *12*, 213–225.
- Hambrey, M. J., N. F. Glasser, B. C. McKelvey, D. E. Sugden, and D. Fink (2007), Cenozoic landscape evolution of an East Antarctic oasis (Radok Lake area, northern Prince Charles Mountains), and its implications for the glacial and climatic history of Antarctica, *Quat. Sci. Rev.*, *26*(5–6), 598–626, doi:10.1016/j.quascirev.2006.11.014.
- Herman, F., F. Beaud, J.-D. Champagnac, J.-M. Lemieux, and P. Sternai (2011), Glacial hydrology and erosion patterns: A mechanism for carving glacial valleys, *Earth Planet. Sci. Lett.*, *310*(3–4), 498–508, doi:10.1016/j.epsl.2011.08.022.
- Hooke, R. L. (1991), Positive feedbacks associated with erosion of glacial cirques and overdeepenings, *Geol. Soc. Am. Bull.*, *103*(8), 1104–1108.
- Jamieson, S. S. R., D. E. Sugden, and N. R. J. Hulton (2010), The evolution of the subglacial landscape of Antarctica, *Earth Planet. Sci. Lett.*, *293*, 1–27, doi:10.1016/j.epsl.2010.02.012.
- Kleman, J., and C. Hättestrand (1999), Frozen-bed Fennoscandian and Laurentide ice sheets during the Last Glacial Maximum, *Nature*, *402*, 63–66.
- Lawson, D. E., J. C. Strasser, E. B. Evenson, R. B. Alley, G. J. Larson, and S. A. Arcone (1998), Glaciohydraulic supercooling: A freeze-on mechanism to create stratified, debris-rich basal ice: I. Field evidence, *J. Glaciol.*, *44*(148), 547–562.
- Marshall, S. J. (2002), Modelled nucleation centres of the Pleistocene ice sheets from an ice sheet model with subgrid topographic and glaciologic parameterizations, *Quat. Int.*, *95–96*, 125–137, doi:10.1016/S1040-6182(02)00033-2.
- Marshall, S. J., and K. M. Cuffey (2000), Peregrinations of the Greenland Ice Sheet divide in the last glacial cycle: Implications for central Greenland ice cores, *Earth and Planet. Sci. Lett.*, *179*(1), 73–90, doi:10.1016/S0012-821X(00)00108-4.
- Molnar, P. (2004), Late Cenozoic increase in accumulation rates of terrestrial sediment: How might climate change have affected erosion rates, *Annu. Rev. Earth Planet. Sci.*, *32*, 67–89, doi:10.1146/annurev.earth.32.091003.143456.
- Pedersen, V. K., D. L. Egholm, and S. B. Nielsen (2010), Alpine glacial topography and the rate of rock column uplift: A global perspective, *Geomorphology*, *122*, 129–139, doi:10.1016/j.geomorph.2010.06.005.
- Roberts, M. J., F. S. Tweed, A. J. Russell, Ó. Knudsen, D. E. Lawson, G. J. Larson, E. B. Evenson, and H. Björnsson (2002), Glaciohydraulic supercooling in Iceland, *Geology*, *30*(5), 439–442.

- Rose, K. C., F. Ferraccioli, S. S. R. Jamieson, R. E. Bell, H. Corr, T. T. Creyts, D. Braaten, T. A. Jordan, P. Fretwell, and D. Damaske (2013), Growth and stability of the East Antarctic Ice Sheet recorded in the landscape of the Gamburtsev Subglacial Mountains, *Earth Planet. Sci. Lett.*, *375*, 1–12, doi:10.1016/j.epsl.2013.03.053.
- Shapiro, N. M., and M. H. Ritzwoller (2004), Inferring surface heat flux distributions guided by a global seismic model: Particular application to Antarctica, *Earth Planet. Sci. Lett.*, *223*(1–2), 213–224, doi:10.1016/j.epsl.2004.04.011.
- Shreve, R. L. (1972), Movement of water in glaciers, *J. Glaciol.*, *11*(62), 205–214.
- Shuster, D. L., K. M. Cuffey, J. W. Sanders, and G. Balco (2011), Thermochronometry reveals headward propagation of erosion in an alpine landscape, *Science*, *332*, 84–88, doi:10.1126/science.1198401.
- Staiger, J. K. W., J. C. Gosse, J. V. Johnson, J. Fastook, J. T. Gray, D. F. Stockli, L. Stockli, and R. Finkel (2005), Quaternary relief generation by polythermal glacier ice, *Earth Surf. Processes Landforms*, *30*, 1145–1159, doi:10.1002/esp.1267.
- Strahler, A. N. (1952), Hypsometric (area-altitude) analysis of erosional topography, *Geol. Soc. Am. Bull.*, *63*(11), 1117–1142, doi:10.1130/0016-7606(1952)63[1117:HAAOET]2.0.CO;2.
- Sugden, D. E. (1978), Glacial erosion by the Laurentide Ice Sheet, *J. Glaciol.*, *20*(85), 367–391.
- Thomson, S. N., M. T. Brandon, J. H. Tomkin, P. W. Reiners, C. Vásquez, and N. J. Wilson (2010), Glaciation as a destructive and constructive control on mountain building, *Nature*, *467*(7313), 313–317.
- Thomson, S. N., P. W. Reiners, S. R. Hemming, and G. E. Gehrels (2013), The contribution of glacial erosion to shaping the hidden landscape of east Antarctica, *Nat. Geosci.*, *6*(3), 203–207, doi:10.1038/ngeo1722.
- Wilson, D. S., S. S. R. Jamieson, P. J. Barre, G. Leitchenkov, K. Gohl, and R. D. Larter (2012), Antarctic topography at the Eocene-Oligocene boundary, *Palaeogeogr. Palaeoclimatol. Palaeoecol.*, *335*, 24–34, doi:10.1016/j.palaeo.2011.05.028.
- Wolovick, M. J., R. E. Bell, T. T. Creyts, and N. Frearson (2013), Identification and control of subglacial water networks under Dome A, Antarctica, *J. Geophys. Res. Earth Surf.*, *118*, 140–154, doi:10.1002/2012JF002555.
- Zachos, J., M. Pagani, L. Sloan, E. Thomas, and K. Billups (2001), Trends, rhythms, and aberrations in global climate 65 Ma to the present, *Science*, *292*(5517), 686–693.
- Zachos, J. C., G. R. Dickens, and R. E. Zeebe (2008), An early Cenozoic perspective on greenhouse warming and carbon-cycle dynamics, *Nature*, *451*, 279–283, doi:10.1038/nature06588.